Hindawi
Journal of Electrical and Computer Engineering
Volume 2023, Article ID 8404457, 15 pages
https://doi.org/10.1155/2023/8404457

Research Article

An FRLQG Controller-Based Small-Signal Stability Enhancement of Hybrid Microgrid Using the BCSSO Algorithm

Ginbar Ensermu,[1] **M. Vijayashanthi**,[2] **Merugu Suresh**,[2] **Abdul Subhani Shaik**,[2] **B. Premalatha**,[2] **and G. Devadasu**[2]

[1]*Wollega University, Electrical and Computer Engineering Department, Nekemte, Oromia, Ethiopia*
[2]*CMR College of Engineering and Technology, Kandlakoya, Medchal Road, Hyderabad, Telangana, India*

Correspondence should be addressed to Ginbar Ensermu; ginbalem@gmail.com

Received 23 May 2022; Revised 1 November 2022; Accepted 13 January 2023; Published 4 February 2023

Academic Editor: Bhargav Appasani

The development of a network termed microgrid (MG) has been motivated owing to augmentation in renewable energy source (RES) infiltration along with the utilization of enhanced power electronic technologies. Recently, more popularity has been gained by the hybrid MG (HMG). Maintaining the power system's (PS) small-signal stability (SSS) is highly complicated during the energy enhancement of RES. The enhancement of the SSS has been focused on by numerous existing methodologies; however, the optimal solution was not obtained by those methodologies. A new controller with the assistance of bell-curved squirrel search optimization (BCSSO) is proposed to address the aforementioned issue. Initially, for PSs such as photovoltaic (PV), wind turbines, along with fuel cells, a mathematical model is ascertained. Then, in this, the converter design has been developed. The PV's maximum power flow is recognized by maximum power point tracking (MPPT) in the bidirectional switched buck-boost converter (BSBBC), which is utilized in this research, and by utilizing the fuzzy ruled linear quadratic Gaussian (FRLQG), the converters are controlled to assure safe operation along with soft dynamics. By employing the BCSSO, the parameters are modified in this controller which in turn ameliorates the SSS. The experiential evaluation of the proposed system's performance is analogized with the existing methodologies. Consequently, the outcomes confirmed that a better performance was attained by the proposed methodology than the prevailing works.

1. Introduction

Owing to the rise in the utilization of DC sources along with loads, the survey on DC MGs has attracted more attention in the past few years. A group of distributed generators (DG), energy storage systems (ESS), local controllable along with noncontrollable loads are together combined into local distribution systems called MG [1]. Through various kinds of power electronics converters (PEC), all of the above said are joined to a common DC bus [2]. AC-MG, DC MG, along with AC/DC MGs are the "3" types of MGs. It assists in the integration along with the application of large-scale RES and is considered a small PS [3]. The prevailing grid infrastructure, safety, and technologies are incorporated into the AC-MG, and it is a highly adapted configuration. The disadvantages are the necessity for the synchronization of DG and losses due to reactive power circulation [4]. The DC MG has the features of excessive conversion efficiency along with smaller line loss when correlated with the AC-MG [5]. AC along with DC in the same distribution grid is combined into a hybrid AC/DC MG in which the direct amalgamation of AC- and DC-centric renewable energy is provided. The conversion stages along with the energy losses are reduced by HMG. A minimal quantity of interface elements is used devoid of the synchronization of generation along with storage units, as they are directly linked to the AC/DC network [6]. Normally, regarding the technical, economic, and environment is unclear. Please rephrase it for clarity., DG is beneficial [7]. The small-signal oscillations are caused in the distribution systems (DS) owing to suboptimal sizing,

inappropriate type, and the improper location of renewable energy hybrid DGs (REHDG) such as wind as well as PV [8]. Irregular clean energies such as wind along with solar energy are extensively employed, and regarding the distribution of time and resources, these energies are more supportive [9]. The main sources of energy for the traditional power grid are fossil fuels, and it causes the release of carbon dioxide along with dust, alterations in the climates, and the ceaseless exhaustion of fossil fuels [10]. The stability along with control of MG has been a significant topic owing to the augmentation in the exploitation of RES [11, 12].

An essential tool for analyzing the PS's performance when they are subjected to minor disturbances is known as small-signal analysis. Individual subgrids and interlinking converters (ILC) play a big role in the stability of an HMG. Consequently, the significance of converter control methods should not be ignored [13]. Subsequently, the solution for instability is sought by the control scheme [14]. Various forms of stability analysis have received a lot of attention. The influences of control system architectures on stability analyses are unquestionable [15]. Either eigenvalue techniques or frequency domain procedures are utilized to appraise the system's stability. As a result, a guarantee can be given to SSS only, and owing to the existence of large-signal disruptions, system stability cannot be assured [16]. In several MG studies, owing to the significance of stability, the power converter controllers' design that are concentrated on preserving and/or increasing the system stability has turned into a focal point [17]. There are numerous literature works on frequency control that are centered on the heuristic optimization method, and they predominantly examine the traditional thermal, hydro-PSs which contain load variation disturbance [18]. The ideas and practices employed for the traditional PSs are insufficient for the MGs along with PSs' stability evaluation with a higher level of linked DGs [19]. So, this paper provides new ways to enrich the MHG's stability and to unravel the inconvenience and challenges regarding the stability.

The paper's remaining part is structured as follows: the prevailing work pertinent to the SSS is examined in Section 2, the proposed system is discussed in Section 3, with the prevailing methodologies, the proposed methodology's performance is analyzed in Section 4, and the paper's future work is listed in Section 5.

2. Related Work

Haseena Kuttomparambil Abdul khader [20] used a metaheuristic hybrid algorithm to present a Type-2 fuzzy fractional-order PID (T2FFOPID) centered PSS, which promoted the power device's electromechanical oscillation damping performance to enrich the dynamic steadiness. In opposition to a huge variety of device fluctuations found in the MG, the massive bandwidth, reminiscence impact, along with flat phase contribution in the frequency reaction of FOPID were formulated to craft the controller and were executed nicely. From a hybrid algorithm, the amalgamation of a dynamic genetic with a bacteria foraging approach, initially, and the T2FFOPID's parameter tuning trouble were changed [21]. Via nonlinear time domain simulations along with performance indices underneath variant disturbances along with working criteria, the controller's functionality in the lower-frequency oscillations within the device having numerous MG penetration ratios was examined. The goal feature of the system was that the integral of the time-weighted absolute of the error (ITAE) had a superior convergence time, and hence, it could have an impact on the device's performance.

Yi Zhang et al. [22] facilitated a network of AC/DC MGs in an adaptively coordinated control strategy (CS) to enrich the system's frequency along with DC voltage, and at the same time, the power-sharing is maintained properly. Initially, the converters linking the AC and DC MGs were produced with the help of a CS on the grounds of a synchronverter along with a virtual DC machine. Except for the power-sharing controller, it contains an adaptive virtual governor along with a virtual inertia regulator. Then, the AC/DC MGs' SSS's evaluation with the offered CS was made to instruct the structure and, in addition, to select the control parameters. Lastly, the technique improved the frequency/DC voltage nadir along with the device's powerful performance, which could be seen through the simulation and investigational outcomes. The optimal values of those parameters were not considered by the adaptive virtual inertia along with a virtual governor gain CS, and so, good performance was not assured [23].

Pankaj Negi et al. [24] analyzed an approach for constructing the control parameters to a voltage source converter and to amplify the steadiness of PV generation in diverse grid capacities, and this strategy is termed as model reference adaptive control (MRAC). A proportional resonant (PR) controller was employed to construct a better damping approach called MRAC, whose gain parameters were adjusted using the ant lion optimization (ALO) algorithm. The LCL filter, PR current, and grid-connected PV, controllers along with their parameters, particularly proportional as well as resonant gains, were primarily concentrated. Additionally, to appraise the controller's functional situation for diverse gain parameters, the phase margin along with the controller transfer functions' gain was developed using an abode plot. Moreover, for optimizing the controller's parameters and stabilizing the device with zero steady-state error, a vast variety of control approaches were made compulsory. With the prevailing controllers, the acquired outcomes and the consequences of the enhanced MRAC approach were compared [25, 26]. The enhanced MRAC strategy's outcomes were provided, and its efficacy was correlated with certain prevailing controllers. Due to its long run time, local optima stagnation, together with premature convergence, and the ALO algorithm could damage the system's performance.

Fan Feng et al. [3] targeted to augment the steadiness of the dual active bridge (DAB) converter-centered ESSs by developing two impedance compensation techniques. Initially, by considering the steadiness of DAB-based ESSs, the layout of the DAB converter's standard feedback controllers was revisited. To resolve the unsteadiness deficiency of the DAB-centric ESS, the optimized design procedures for the

DAB feedback controller were used, which did not need any extra passive components or active control loops [27, 28]. Next, to alter the DAB converter's input impedance, "2" types of impedance shaping regulators (ISRs), such as the bus voltage-centric ISR (BV-ISR) and the bus current-centered ISR (BC-ISR), were utilized. Ultimately, the investigational outcomes confirmed the competence of the optimized DAB controller along with ISRs. But, under all load circumstances, the performance was not verified.

Hossein Shahsavari and AlirezaNategh [29] developed an optimal fractional-order PID controller to expand the probabilistic SSS of the power networks by contemplating the variability of system operating situations while analyzing the consequences of higher infiltration of PV power plants using mathematical techniques. This paper exhibited the principle modules as well as the mathematical illustration of the larger-scale PV generation included with the single-machine infinite-bus PS. Next, an efficient methodology was introduced which revamps the PS stabilizers (PSS) and was robust enough to restrain electromechanical oscillations in power devices that integrate a random PV power [30, 31]. So, this led to the construction of a vigorous PSS centered on the controller's hybridization along with a nondominated sorting genetic algorithm (NSGAII). The NSGAII-based controller's performance was appraised underneath several solar irradiances, temperature settings, together with disturbances. As of the simulation outcomes, it was evident that the system was utilized for developing indispensable controllers for larger scale PV power plants. Only for certain circumstances, the system stabilized the signals [32].

Hassan Pourvalisouraki et al. [33] enforced a DC- AC HMG system to achieve stable responses in steady-state and dynamic operations, by devising a diverse control approach. To construct the controller, the small-signal linearization (SSL) technique and the direct Lyapunov method were merged. Different from other existing Lyapunov-centered methods, the controller's the steady-state components were derived using SSL-based mathematical terms [34, 35]. The various contributions to the control method's structure are (a) controlling the PCC voltage frequency along with DC-link voltage errors directly; (b) more efficient DC/AC converter current decoupling features; and (c) the bidirectional DC/DC converter can be supervised directly by the input voltage error [36]. Lastly, relative MATLAB/simulink simulation outcomes were offered to publish the superiority of the prevailing controller united with SSL underneath AC/DC load variations, storage unit's discharging/charging, and the sharing of AC loads amongst grid sides together with DC sources [37]. In the Lyapunov theory, the initial polynomial functions were very intricate, which could impact the system's running time.

3. Small Signal Stability Enhancement Using the Novel Controller with the Evolutionary Algorithm

For distributed renewable energies linking to the utility grid, the MG is considered an effectual conception. Nevertheless, the study of MG has faced numerous challenges. The instability is the major issue in the HMG. A novel evolutionary algorithm centered on SSS advancement in DC-AC HMG is proposed here to conquer this complication. Firstly, the hybrid energy resources' mathematical model is procured. Then, to control the converter's operation, the BSBBC is designed; in addition, the FRLQG controller is utilized in this methodology. The BCSSO, which ameliorates the system's stability, is utilized to tune the controller's parameters. Figure 1 shows the proposed methodology's block diagram.

3.1. Mathematical Model of Distributed Renewable Energies. Initially, for wind turbines, PV arrays, batteries, along with fuel cells, the mathematical model is recognized.

3.1.1. Mathematical Model for PV Arrays. Sunlight is transmuted into electricity by the PV system. The photovoltaic cell is the PV system's fundamental component. The PV cell's characteristics are identical to the normal diode in the dark. The electrons are set free, whilst the cell is hit by sunlight with energy higher than the semiconductor energy gap; thus, an extensive current flows in the external circuit. PV cells are grouped into modules, encapsulated as of the front, and backed by a metallic panel for protection since they are fragile along with lower voltage. PV's mathematical formulation is as follows:

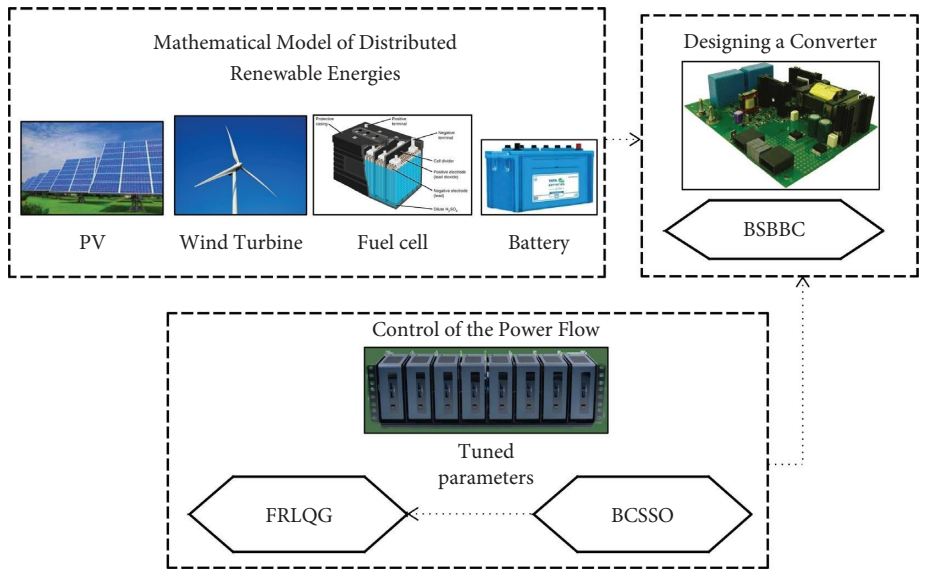

Figure 1: Block diagram for the proposed research methodology.

$$
\begin{aligned}
C(U,S,A) &= C_{ph} - C_o\left(e^{(A+CR_s)/nA_{th}} - 1\right) - \frac{(A + C \cdot R_s)}{R_{sh}} = C_{ph} - C_D - C_{sh},\\
C_{ph} &= C_{ph_o} \cdot \frac{S}{S_{\text{nom}}},\\
C_{ph}(U) &= C_{ph} + K_o(U - U_{\text{meas}}),\\
K_o &= \frac{\left(C_{ph}(U_2) - C_{ph}(U_1)\right)}{(U_2 - U)},\\
C_o &= C_{sc(U_1)} \cdot \left(\frac{U}{U_1}\right)^{3/n} \cdot e^{\left[-E_g/P_s\left(1/U_1(U-1)\right)\right]},\\
C_o(U_1) &= \frac{C_{SC(U_1)}}{\left(e^{qA_{OC(U_1)}/nkU_1} - 1\right)},\\
R_s(U) &= \frac{-dA}{dC_{A_{OC}}} - \frac{1}{\left(C_{o(U_1)} \cdot q/nkU_1 \cdot e^{qA_{OC(U_1)}/nkU_1}\right)},\\
R_{sh} &= \frac{A_{OC}}{\left[C_{ph} - C_o\left(e^{qA_{OC}/nkU_{\text{meas}-1}}\right)\right]},\\
R_{sh}(U) &= R_{sh} \cdot \left(\frac{U}{U_{\text{meas}}}\right)^{\alpha},
\end{aligned}
\tag{1}
$$

where the photo-generated current in amperes is specified as C_{ph}, the photo-generated current at the nominal radiation is signified as C_{ph_o}, the diode dark saturation current is denoted as C_o, the diode dark current is represented as C_D, the shunt current is illustrated as C_{sh}, the series resistance is indicated as R_s, the shunt resistance is defined as R_{sh}, the solar radiation in w/m^2 is proffered as S, the S_{nom} is the radiation, the photo voltaic module standardized at the ideality factor is denoted as e, the electron charge is indicated as k, Boltzmann's constant is specified as P_g, the semiconductor energy gap is denoted as K_0, the short-circuit current temperature coefficient is represented as q, the electron change is defined as E_s, the number of cells in series is signified as E_s, the short-circuit current is illustrated as C_{sc},

the open-circuit voltage is defined as A_{OC}, and the thermal voltage is proffered as A_{th}, which is expressed as follows:

$$A_{th} = \frac{nkU_c}{e}. \tag{2}$$

3.1.2. Mathematical Model of Wind Turbine. The wind turbine-generated power relies on wind speed. The algebraic sum of gust wind speed (WS), base WS, and noise WS, along with ramp WS is termed the wind. The wind turbine's mechanical power is as follows:

$$M_m = 0.5\rho W_a \overline{PC_p} v_{sw}^3, \tag{3}$$

where the mechanical power in watts is specified as M_m, the air density (kg/m^3) is signified as p, the swept area (m^2) is denoted as W_a, the turbine power coefficient is represented as $\overline{PC_p}$, and the WS (m/s) is indicated as v_{sw}. The turbine conversion efficiency is represented by the power coefficient. If the pitch angle $B = 0$, then the tip speed function is denoted as $\overline{PC_p}$, and the turbine's conversion efficiency is indicated as δ and is expressed as follows:

$$\overline{PC_p}(\delta) = c_1\left(\frac{c_2}{\delta} - c_4\right)e^{-c_5/\delta} + c_6\delta, \tag{4}$$

where

$$\delta = \frac{\omega B_r}{v_{sw}}, \tag{5}$$

where the coefficients are given as c_1, c_2, c_4, c_5, and c_6, the rotational speed (rad/s) is indicated as w, and the blades' radius is specified as B_r.

3.1.3. Mathematical Model for Fuel Cells. The fuel cell is a device in which electricity is generated as of the chemical reaction of hydrogen along with oxygen. The fuel cells' mathematical model is as follows:

$$\begin{aligned} F_{OC} &= k_c F_n, \\ CT_0 &= \frac{zHL\left(I_{H_2} + I_{O_2}\right)}{Lh} e^{-\Delta G/LU}, \\ Vol &= \frac{Lu}{z\gamma H}, \end{aligned} \tag{6}$$

where the Nernst voltage is defined as F_n, the voltage constant at nominal conditions is indicated as k_c, the number of moving electrons is represented as z, the energy values are symbolized as H, L, the partial pressure of hydrogen is explained as I_{H_2}, the partial pressure of oxygen is represented as I_{o_2}, Plank's constant is defined as h, the size of the activation barrier is signified as ΔG, the temperature is represented as U, and the charge transfer coefficient is specified as γ.

3.1.4. Battery System Modelling. When the system has power deficiency, batteries that store surplus power in the HPS are utilized. The number of times the battery is charged/discharged in a day specifies the battery's lifetime.

$$BTT = C + M_m + F_{OC} - \overline{CC_l}, \tag{7}$$

where the battery is indicated as BTT and the hybrid DC and AC dynamic load is denoted as $\overline{CC_1}$. The remaining power is stored in the battery following the AC and DC load.

Figure 2 shows the HMG structure. In this, AC loads are linked in the AC bus; similarly, in the DC bus, the battery PV, DC loads, along with fuel cells are connected.

3.2. Proposed Algorithm. In this section, the electrical energy flow is processed along with a controlled converter by providing voltages and currents in a way, which optimally suits the loads. The BSBBC (bidirectional converter) is utilized here. It has the potency to obtain the required output voltage in both directions of power flow by boosting the input voltage in a single stage. For the intermediate network betwixt lower voltage DC and the converter leg, "1" capacitor, "2" relays, "1" inductor, "3" active switches, and "1" diode are utilized here. On the AC along with the DC bus energy status, the direction of power flow is dependent upon, and also, it is centered on the direction of power flow switches that are being operated. In the AC bus as well as the DC bus, the frequency of deviation in energy status is utilized to be lesser; thus, the switches' one part is employed as relays. Higher-frequency control switches are considered as the other part of the switches. These switches are functional regarding the shoot through duty ratio to control the voltage gain in the inverting mode along with the rectifying mode. To discover the maximum power as of the PV module under variable temperatures along with shading conditions, there is a necessity for the development of the MPPT. Furthermore, the FRLQG controls all the converters to assure safe operation along with soft dynamics. It is an amalgamation of fuzzy rules and linear quadratic control. In the linear quadratic control, the problem of poor tracking performance may be caused owing to the consumption of extra power; thus, the fuzzy rules are utilized in this methodology regarding which the controller is executed. The main objective is to minimize the operating cost of the consumed energy by a microgrid. The algorithm was developed to find the optimal operating set-points for which a power system control is required to maintain a continuous balance between power generation and load demand. The load frequency controller and automatic voltage regulator play an important role in maintaining constant frequency and voltage in order to ensure the reliability of electric power. In order to improve the performance and stability of these control loops, proportional-integral-derivative (PID) controllers are normally used. But these fixed gain controllers fail to perform under varying load conditions and hence provide poor dynamic characteristics with a large settling time, overshoot, and oscillations. In order to achieve better dynamic performance, system stability, and sustainable utilization of generating systems, controller parameters must be well-tuned. In this paper, evolutionary algorithms are proposed to find the optimum parameters of the controller

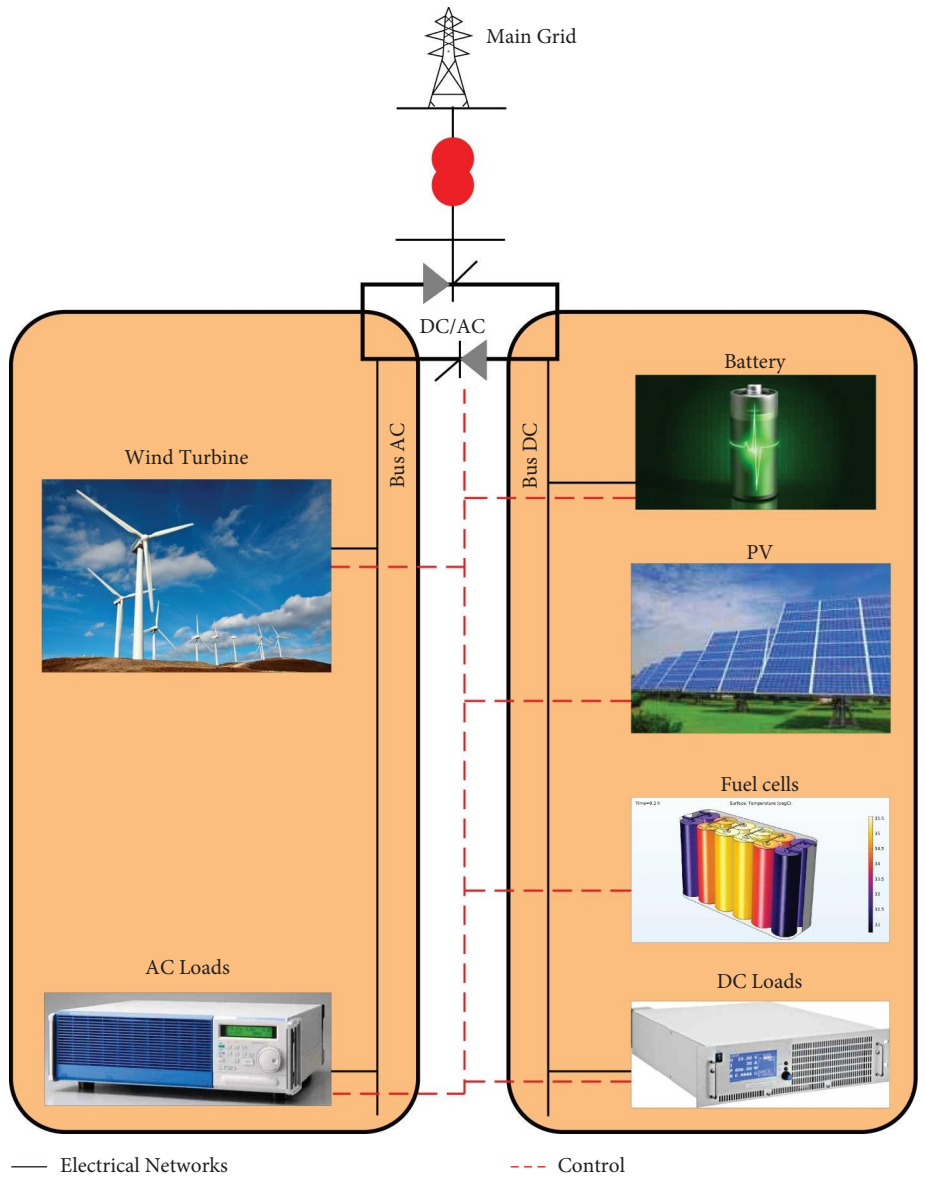

Figure 2: Structure of a hybrid microgrid.

to control the voltage and frequency of the generating system within the permissible limit. These algorithms offer a more stable and faster convergence towards the best parameters and also with minimum computational time. These algorithms are appropriate to model the uncertainties found in the power demand and improve the flexible nature of the controllers.

The plant's state-space model is

$$X(t) = O_m X(t) + I_m v(t) + \xi_1 a(t), \tag{8}$$

$$Y(t) = O_m X(t) + \xi_2 \overline{a}(t). \tag{9}$$

Here, X communicates to the state vector, the contribution aimed at the framework is signified as v, and the deliberate output as of the ideal plant is defined as Y, together with a specifies the Gaussian repetitive disturbance following up on the framework; the system matrix, the input matrix, and the output matrix are represented as S_m, I_m, and O_m; the noise matrices are denoted as ζ_1 and ζ_1. In this, to control the battery charging/discharging current, the fuzzy logic is implemented. $X(t)$ and $Y(t)$ are the parameters estimated by a set of fuzzy rules of the form:

If ΔO_m is ω_i and $\Delta(\Delta O_m)$ is ω_i, then

$$\begin{aligned} X(t) &= J_i, \\ Y(t) &= Q_i, \end{aligned} \tag{10}$$

where $\bar{\omega}_i$, ω_i, J_i, and Q_i are fuzzy sets on the respective supporting sets.

The fuzzy membership function(MF) sets are offered as triangular partitions in the FRLQG; positive small (PS), positive big (PB), negative big (NB), zero (ZO), and negative small (NS) are the partitions. To ameliorate the SSS and to augment the methodology's performance, the controller's

parameters are tuned before controlling the power flow. The BCSSO algorithm is utilized here. Southern flying squirrels' dynamic foraging behavior through gliding is imitated by the squirrel search optimization (SSO) algorithm. It is also an effective approach utilized by small mammals for traveling long distances in the deciduous forests of Europe as well as Asia. Acorn nuts are effortlessly found by them to meet their everyday energy requirements. The following phases illustrate the SSO mathematically regarding the flying squirrels' food foraging strategy. In general, SSO, regarding the uniform distribution, the random value is chosen which devalues the performance because numerous chances are there to choose the worst optimal resolution at this random selection. Thus, a bell-shaped constant centered on the Cauchy distribution function is utilized in this research. Parameter initialization, random initialization of flying squirrel locations, sorting, declaration, random selection, generating new locations, and inspecting seasonal conditions are the steps included in this algorithm. In this, the squirrels are regarded as the controller parameters.

3.2.1. Initialization of the Parameters. The SSA major parameters are the population size P_s, the maximum number of iteration ma_i, the predator presence probability py_i, the number of decision variables X, the gliding constant Φ, the scaling factor s_f, along with the upper and lower bounds for the decision variable are ψ_u as well as ψ_1. At the beginning of the SSA procedure, these parameters are set.

3.2.2. Random Initialization of Flying Squirrel's Locations. In a forest, there are n_n flying squirrels (η); thus, the squirrels are regarded as the input parameters. The i^{th} flying squirrel's location on the i^{th} tree is specified by a vector,

$$\eta_{i,j} = (\eta_{i1}, \eta_{i2}, \eta_{i3}, \ldots\ldots\ldots, \eta_{id}), \quad i = 1, 2, 3, \ldots\ldots, n_n, \tag{11}$$

where the i^{th} flying squirrels of the j^{th} dimension are denoted as η_{ij} and the number of dimensions is indicated as d. After that, in the search space, the flying squirrels' locations are initialized randomly as follows:

$$\psi_{i,j} = \psi_l + B_s * (\psi_u - \psi_l), \quad i = 1, 2, \ldots\ldots, P_s,\ j = 1, 2, \ldots\ldots, n_n, \tag{12}$$

wherein a bell-curved number is specified as B_s and this is derived by utilizing the Cauchy distribution function. Next, for the optimized controller, the fitness function (FF) is analyzed. The FF is regarded as the maximization of the SSS along with the minimization of the quadratic cost functions (QCFs). The enhancement of SSS's objective function is as follows:

$$\max(\kappa_i), \tag{13}$$

where the SSS term is denoted as κ_i. The optimal LQG design starts with a model in the form of equations (18) and (19). In this, the process noise is described as $a(t)$, and the measurement noise is illustrated as $\overline{a}(t)$. In the optimal LQG, the feedback control is built to mitigate the following QCF,

$$\mathrm{QCF} = \lim_{T \longrightarrow \infty} EV \frac{1}{T} \int_0^T \left(X(t)^T\ FX(t) + v(t)^T RRv(t) \right).\mathrm{d}t. \tag{14}$$

Here, symmetric weighting matrices are specified as $F \geq 0$ and $RR \geq 0$, and the expected value is denoted as $EV[\cdot]$. To limit the control inputs' states along with size, the terms $X^T FX$ and $v^T RRv$ are analogized to a prerequisite in (14). In the cost function, the selection of the matrices F and RR relies on the system's required performance. The robustness problems against the plant uncertainty are not addressed directly by the controller's design. The LQG's robustness is leaned by the noise's considerable decision regarding the plant model equations (18) and (19), which reflects the required bandwidth along with robustness characteristics. In this, mitigating the tracking error among the command signal along with the gauged output is the control objective. To execute this, an IC is related to an SN system owing to its phenomenal lower-frequency tracking operation. Tracking errors are reduced by the higher gain of the IC even though it displays a lower bandwidth, which proves the robustness insufficiency. Therefore, $f = (f_1, f_2, \ldots, f_{P_s})$ denotes the fitness value (FV) derived. An individual flying squirrel's location's FV is gauged by substituting the decision variables' value into a FF:

$$f_i = f_i\left(\psi_{i,1}, \psi_{i,2}, \ldots, \psi_{i,n_n}\right), \quad i = 1, 2, \ldots, P_s. \tag{15}$$

3.2.3. Sorting, Declaration, and Random Selection. All the FS position FVs are sorted in ascending order. It is observed that the squirrel with the minimal FV is on the hickory nut tree (optimal food source), the next "3" best flying squirrels are on the acorn tree (normal food source), and the remaining squirrels are on the normal trees (no food source). Moreover, by executing randomized selections, some FSs are believed to fly toward the direction of the hickory nut tree concerning that the squirrels have got satisfied with their daily energy requirements. The remaining FSs are glided towards the acorn nut tree.

3.2.4. Generation of New Locations. There occurs "3" situations in the nonexistence of a predator at the time of the dynamic forging of flying squirrels. In this, the flying squirrel glides together with searches all over the forest for its favorite food. However, the flying squirrel is watchful; in addition, it is forced to take a small random walk to search for the closest hiding location. The dynamic foraging behavior "3" mathematically modeled cases are given as follows:

(a) Flying squirrels on acorn nut trees (ψ_{at}) may move towards the hickory nut tree. Here, the squirrels' new location is acquired as follows:

$$\eta_{ct}^{t+1} = \begin{cases} \eta_{ct}^t + gl_d.ls_c.\left(\eta_{kt}^t - \eta_{ot}^t\right), & \text{if}, r_1 \geq pp_p, \\ \mathrm{ran}_l, & \text{otherwise.} \end{cases} \tag{16}$$

Here, the flying squirrel location on the acorn tree at t and $t+1$ iteration is specified as η_{ct}^t and η_{ct}^{t+1}, the

gliding distance is indicated as gl_d, the sliding constant is represented as ls_c, the flying squirrel on the hickory tree is indicated as η_{kt}, the flying squirrel on a normal tree is described as η^t_{ot}, the random number in the range of [0, 1] is denotes as r_1, the predator presence probability is signified as pp_p, and the random location is represented as ran_i.

(b) To accomplish their daily energy requirements, ψ_{nt} may move towards acorn nut trees. The squirrels' new location is updated as follows:

$$\eta^{t+1}_{ot} = \begin{cases} \eta^t_{ot} + gl_d.ls_c.\left(\eta^t_{ct} - \eta^t_{ot}\right), & \text{if}, r_2 \geq pp_p, \\ \mathrm{ran}_l, & \text{otherwise.} \end{cases} \quad (17)$$

Here, the flying squirrels' location on the normal tree at t and $t+1$ iteration is represented as η^{t+1}_{ot}, and the random number 2 is indicated as r_2, which existed in the range of [0, 1].

(c) To store the hickory nuts for consuming them when there is a shortage of food, few FS as of the normal trees, which have already consumed acorn nuts, might glide in the hickory nut tree's direction. Here, the FS updated positions are obtained utilizing the following equation:

$$\eta^{t+1}_{ot} = \begin{cases} \eta^t_{ot} + gl_d.ls_c.\left(\eta^t_{kt} - \eta^t_{ot}\right), & \text{if}, r_3 \geq pp_p, \\ \mathrm{ran}_l, & \text{otherwise.} \end{cases} \quad (18)$$

Here, the random number 3 presented in the range of [0, 1] is represented as r_3.

3.2.5. Check Seasonal Condition Monitoring. The flying squirrel foraging activity has got affected significantly by seasonal changes. Therefore, the changes in weather affect the flying squirrels movement, and a highly realistic approach towards optimization is provided by the addition of such behavior. Consequently, the solution is prevented as of the local optimal solutions by monitoring the seasonal condition. Initially, the seasonal constant sea_c is computed as follows:

$$\mathrm{sea}^t_c = \sqrt{\sum_{j=1}^{d} \left(\eta^t_{ct,j} - \eta^t_{kt,j}\right)^2}, \quad (19)$$

where the seasonal constant at iteration t is specified as sea^t_c, the squirrel on the hickory and acorn trees at j^{th} dimension is signified as $\eta^t_{kt,j}$ and $\eta^t_{ct,j}$, and the total dimension is represented as d. Subsequently, in the 2nd step, the seasonal monitoring criterion is checked by $\mathrm{sea}^t_c < \mathrm{sea}_{\min}$ in which the seasonal constant minimum value is represented as $\mathrm{sea}_{\min}$, and it is calculated as follows:

$$\mathrm{sea}\frac{10e^{-6}}{(365)^{t/\left(t_{\max}/2.5\right)_{\min}}}, \quad (20)$$

where the maximum number of iterations is indicated as $t_{\max}$. The end of the winter season is found if the seasonal condition is true; thus, the flying squirrels, which lose their potency to travel around the forest, will randomly transfer their searching positions for food sources over again.

$$\eta^{t+1}_{ot} = \eta_{\downarrow} + ev_y \times \left(\eta_{\uparrow} - \eta_{\downarrow}\right), \quad (21)$$

where the levy distribution function is denoted as ev_y. It promotes better search space exploration and is computed as follows:

$$ev_y = 0.01 \times \frac{\tau_a \times \sigma}{\left|\tau_b\right|^{1/\varepsilon}}, \quad (22)$$

where the "2" normally distributed random numbers in the range [0, 1] are represented as τ_a and τ_b, a positive constant is defined as ∂, which is lesser than 2, and σ is computed as follows:

$$\sigma = \left(\frac{\Gamma(1+\varepsilon) \times \sin(\pi\varepsilon/2)}{\Gamma(1+\varepsilon/2) \times \varepsilon \times 2^{(\varepsilon-1/2)}}\right)^{1/\varepsilon}, \quad (23)$$

where the factorial function is denoted as Γ (Algorithm1).

3.2.6. Pseudocode for the Proposed BCSSO Algorithm. The BCSSO's pseudocode is demonstrated. The parameter initialization, fitness analysis along with the updating process for the squirrel locations are explicated.

4. Results and Discussion

The proposed SSS enhancement of the HMG's performance is assessed here. The proposed system is executed in MATLAB/simulink shown in Figure 3.

4.1. Performance Analysis. In this, the phase of the proposed system along with its magnitude is evaluated; subsequently, the frequency of the system with and without tuning the controller's parameters is appraised.

The present controller phase behavior evaluation is depicted in Figure 4. The controller phase is altered regarding the frequency. In this, the frequency level is regarded as of 10^{-3} to 10^3 rad/s. The controller is presented at -90° at the 10^{-3} frequency, and then, after 10° frequencies, the phase is completely altered.

The controller's magnitude is displayed in Figure 5. Regarding the frequency, the magnitude is altered. The controller's magnitude is different for varied frequencies. The controller has the 30 dB, 60 dB, and 90 dB magnitude for frequencies above 10°; similarly, the controller has −30 dB, −60 dB, and −90 dB magnitudes for frequencies below 10°.

The frequency evaluation with and without tuning the controller's parameter is exhibited in Figure 6. Regarding the time variation, the frequency is assessed. When the time is 0.1 sec, the light deviation occurred whilst tuning the controller's parameters, whereas a higher level frequency variation occurred without tuning the controller's parameters. Consequently, it is confirmed that better outcomes are obtained by tuning the controller's parameters than without the tuning of the controller's parameters.

Input: parameters (t) and Y (t)
Output: optimal parameters
Begin
Initialize location $\eta_{ij} = (\eta_{i1}, \eta_{i2}, \eta_{i3}. \ldots \ldots \ldots \eta_{id})$ seasonal constants sea_c^t and maximum Iteration Max_u
Define initial location of each flying squirrel by, $\psi_{ij} = \psi_l + Bs * (\psi_u - \psi_l)$
Calculate fitness function
Set iteration $II_t = 1$
While $(II_t \leq Max_{it})$ do
Generate locations using 3 locations
Scenario 1:
If $(r_1 \geq pp_p)$; {
Update the squirrel location $\eta_{ct}^t + gl_d .ls_c (\eta_{kt}^t - \eta_{ot}^t)$
} else {
$\eta_{ct}^{t+1} = ran_l$
}
end if
Scenario 2
If $(r_2 \geq pp_p)$; {
Update the squirrel location $\eta_{ot}^t + gl_d .ls_c (\eta_{ct}^t - \eta_{ot}^t)$
} else {
$\eta_{ot}^{t+1} = ran_l$
}
end if
Scenario 3
If $(r_3 \geq pp_p)$; {
Update the squirrel location $\eta_{ot}^t + gl_d .ls_c (\eta_{kt}^t - \eta_{ot}^t)$
} else {
$\eta_{ot}^{t+1} = ran_l$
}
end if
Perform seasonal monitoring by using a seasonal constant
Calculate fitness function
Set $II_t = II_t + 1$
End while
Return optimal parameters

Algorithm 1: Bell-curved squirrel search optimization (BCSSO) algorithm.

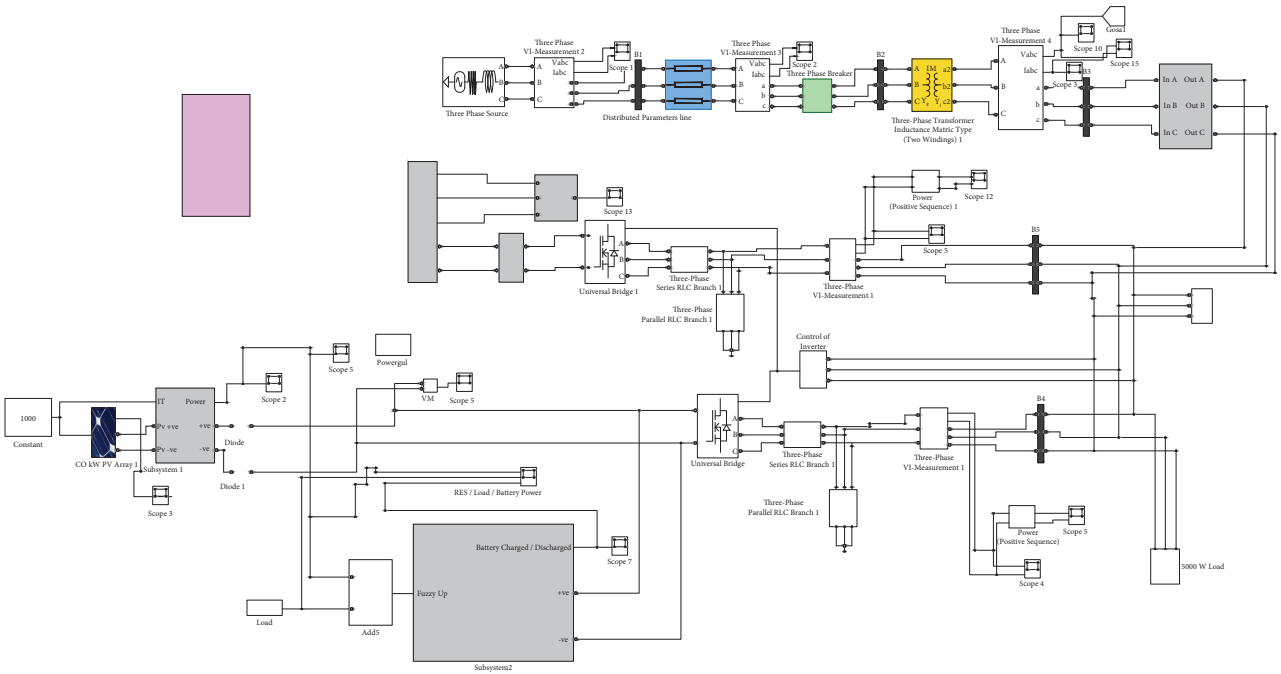

Figure 3: The MATLAB/simulink model of HMG with the PV, battery, and fuel cell.

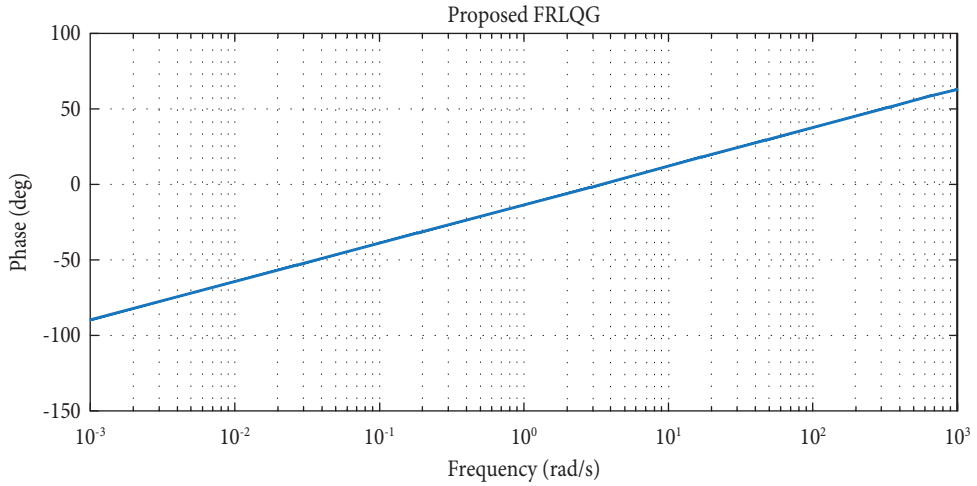

Figure 4: Analysis of the phase behavior of the controller.

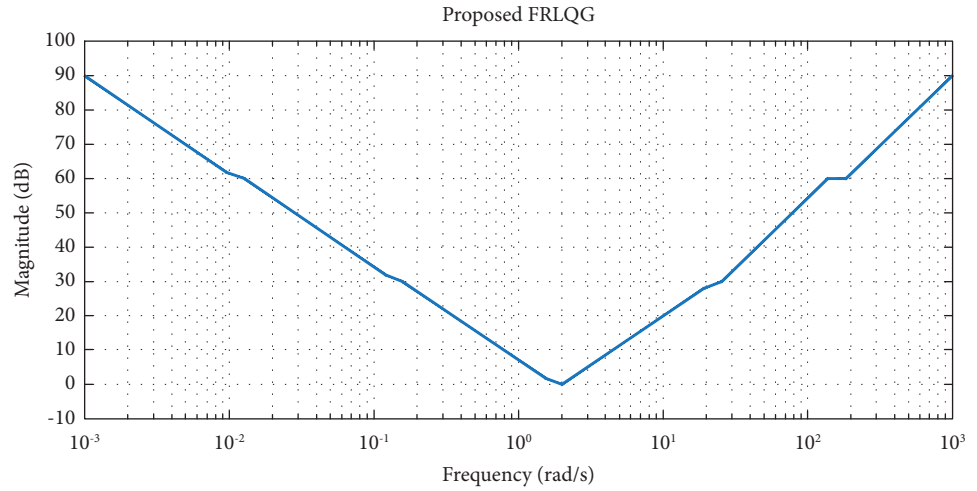

Figure 5: Analysis of the magnitude of the controller.

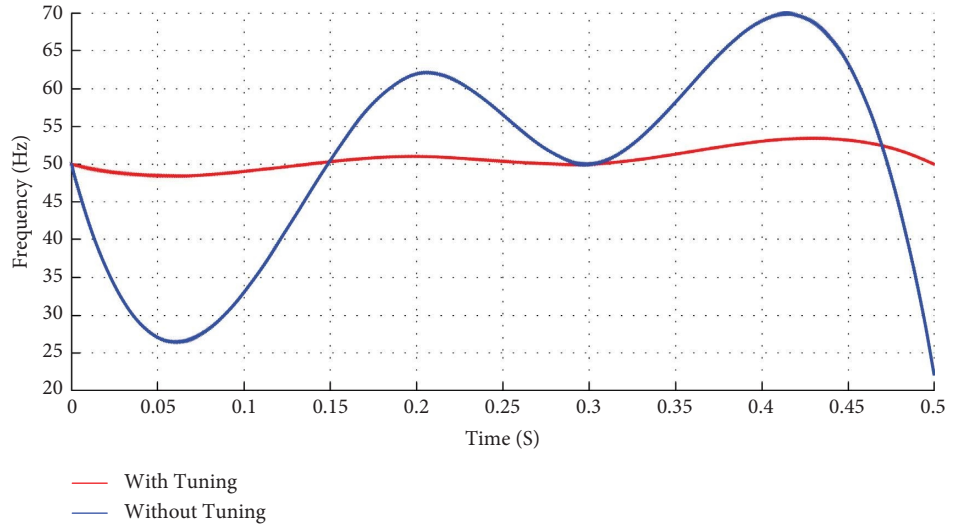

Figure 6: Frequency analysis.

4.2. Comparative Analysis. The performance of the proposed controller and the prevailing PID controller and the proportional integral (PI) controller is assessed regarding the voltage evaluation. Next, by tuning the controller's parameter, the BCSSO-centered FRLQG controller is analogized with the prevailing evolutionary algorithm-centered controllers such as particle swarm optimization-FRLQG (PSO-FRLQG), SSO-FRLQG, and genetic algorithm-FRLQG (GA-FRLQG) regarding the QCF, stability, along with speed deviation. Finally, regarding the fitness evaluation, the performance of the proposed evolutionary algorithm and the existing PSO, SSO, and GA is analogized.

Figure 7 illustrates the controlled switching signal voltage comparison meant for the FRLQG and the prevailing LQG, PID, and PI controllers. Regarding the time in seconds, the voltage gain is assessed. The voltage gain at time 0.2 sec is 355 V for the proposed controller and 212 V and 185 V for the prevailing controllers. Likewise, at time 0.3 sec, the proposed system has the 303 V, and the prevailing LQG, PID, and PI controllers have obtained 202 V, 196 V, and 174 V, respectively. For the remaining time seconds also, a better outcome is acquired by the proposed than the existent controller. Therefore, the proposed systems' better performance is proved.

The speed deviation of the proposed and the existent controller is evaluated in Figure 8. The frequency regulation is centered on the speed control of all generators joined to the grid; thus, the speed deviation evaluation is a significant procedure. Regarding time seconds, the speed deviation is varied. As of the evaluation, it is perceived that a higher-speed deviation is experienced by the previous GA-FRLQG than the other existent along with the proposed methodologies all the time. For instance, at time 6 sec, a speed deviation of 1 p.u is possessed by the BCSSO-FRLQG; similarly, speed deviations of 1.2 p.u, 1.5 p.u, and 1.7 p.u are possessed by the prevailing SSO-FRLQG, PSO-FRLQG, and GA-FRLQG, respectively. Thus, a better outcome is attained by the proposed BCSSO-centered FRLQG, and the worst outcome is attained by the prevailing GA-centric FRLQG. Consequently, it is confirmed that a lesser speed deviation is accomplished by the proposed system than by the prevailing controller.

Figure 9 exhibits the QCF evaluation for the tuned controllers. The controller with minimal QCF shows better performance. The proposed controller's QCF value for 0sec is 0, 43%, 49%, 56%, 55%, and 61%, and for 0.5 sec, it is 0.1 sec, 0.2 sec, 0.3 sec, and 0.4 sec. The prevailing controllers have a higher QCF than the proposed system. For example, the QCF for the SSO-FRLQG, PSO-FRLQG, and GA-FRLQG at time 0.5 s is 75%, 77%, and 83%. A higher QCF is attained by the prevailing controllers for the remaining time also. As a consequence, it is confirmed that better performance was attained by the proposed algorithm centric grid design than by the other methodologies.

The system stability enhancement is exhibited in Figure 10. The stability gauge for any dynamic system exposed to smaller perturbations is mentioned as SSS. This research model's major purpose is stability evaluation. The higher stability of 93% is attained by BCSSO-FRLQG at 0.5 sec than

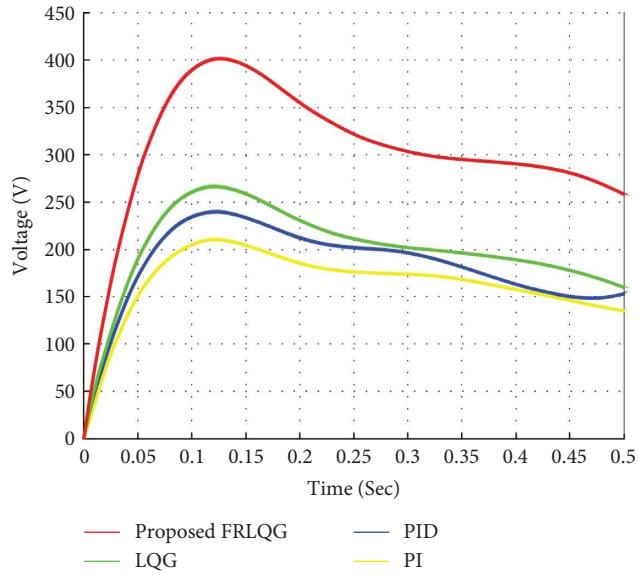

Figure 7: Analysis of voltage.

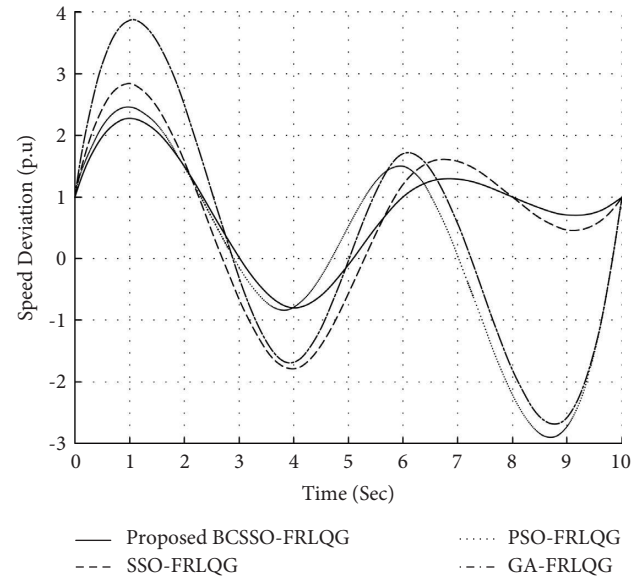

Figure 8: Speed deviation analysis.

the other prevailing SSO-FRLQG, PSO-FRLQG, and GA-FRLQG controllers, which obtained stability of 74%, 67%, and 56%, respectively. For the remaining time seconds also, higher stability is attained by the proposed than the prevailing controller-centered HMG. Hence, it is proved that better performance was acquired by the proposed methodology than by the prevailing methodologies.

Fitness vs. iteration of the BCSSO with the previous SSO, PSO, and GA are depicted in Table 1. A fitness of 0.978 is attained by the BCSSO, and a fitness of 0.906, 0.864, and 0.796 is attained by the prevailing SSO, PSO, and GA for the 25^{th} iteration. A higher fitness is attained by the proposed than the prevailing algorithms. The proposed model attains better fitness than the existent algorithms for the remaining iterations as well. Accordingly, it is proved that a better

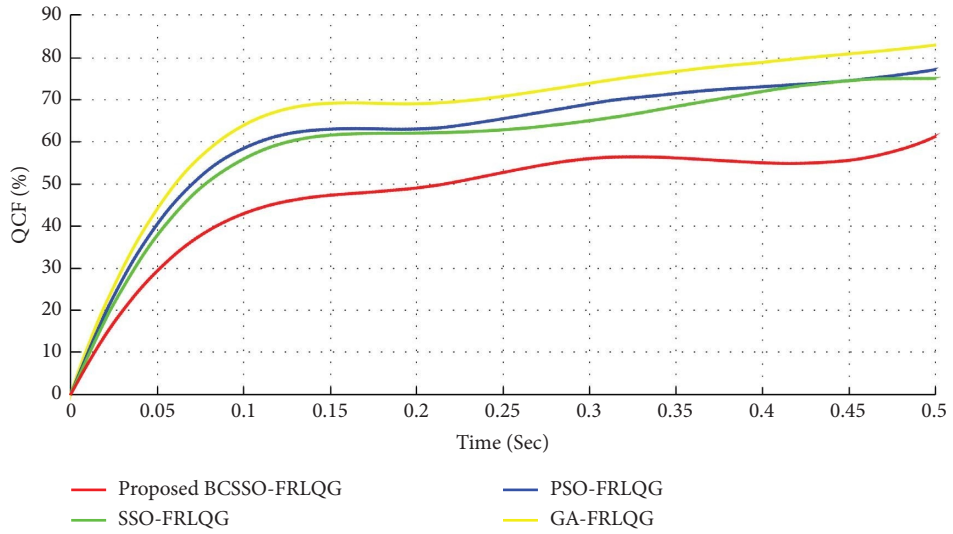

Figure 9: Comparison analysis of tuned controllers based on the QCF metric.

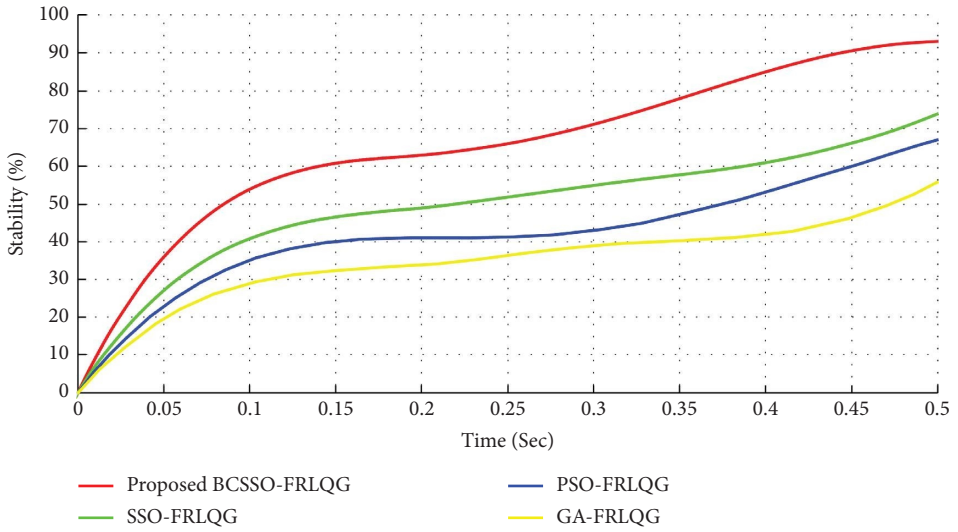

Figure 10: Stability enhancement analysis.

Table 1: Fitness vs. iteration analysis.

Iterations	Proposed BCSSO	SSO	PSO	GA
5	0.721	0.684	0.653	0.613
10	0.796	0.723	0.691	0.634
15	0.831	0.786	0.749	0.696
20	0.901	0.842	0.813	0.753
25	0.978	0.906	0.864	0.796

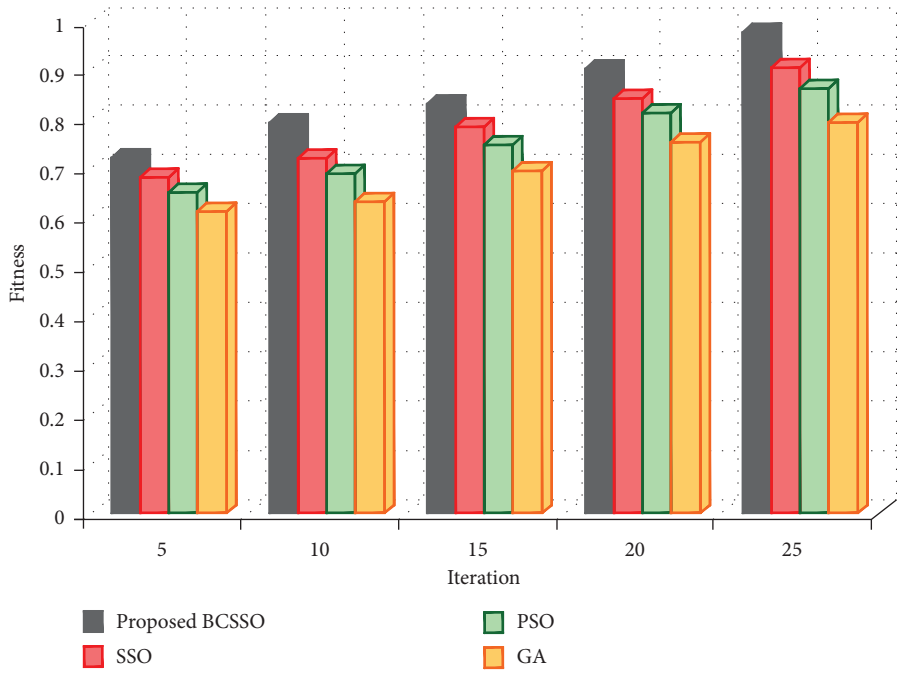

Figure 11: Graphical plot for fitness vs. iteration analysis.

outcome was attained by the proposed evolutionary algorithm. Figure 11 exhibits the graphical plot of fitness vs. iteration analysis.

5. Conclusion

This paper presents a framework for stability analysis and performance evaluation of microgrids. In addition, various parameters and their impacts on the microgrid dynamic performance are investigated. To modify the parameter, a new controller with the BCSSO was proposed here; thus, it meliorated the SSS. Firstly, for hybrid renewable energies, mathematical models are recognized. After that, the converter is designed; in addition, the evolutionary algorithm is utilized to control the power flow. Regarding the phase behavior along with magnitude, the proposed methodologies' performance is assessed. Next, the frequency is evaluated with and without tuning the controller's parameter. In accordance with the evaluation, the best outcomes are obtained by the tuning parameter-centered controller. Then, regarding QCF, speed deviation, along with stability, the performance of the BCSSO- FRLQG controller, and the prevailing PSO-FRLQG, SSO-FRLQG, and GA-FRLQG are analogized. Subsequently, for the proposed work and for the existing converters such as PID, LQG, along with PI, the voltage is evaluated. The comparison outcomes proved that a better outcome along with higher stability was attained by the proposed methodology. A stability of 93% was obtained by the BCSSO-FRLQG at time 0.5 sec, which is higher than the other methodologies. After that, the BCSSO's fitness is assessed with the prevailing evolutionary algorithms; subsequently, it is established that the proposed one attained the best outcome. Therefore, it is recognized that the current converter and controller-centric HMG are highly efficient for PSs to ameliorate the SSS. In the upcoming future, to promote the system performance, the proposed methodology can be advanced with highly renewable energies and enhanced algorithms.

Nomenclature

C_{ph}:	Photo-generated current in amperes
C_{ph_o}:	Photo-generated current at the nominal radiation
C_o, t:	The diode dark saturation current
C_D:	The diode dark current
C_{sh}:	The shunt current
R_s:	The series resistance
R_{sh}:	The shunt resistance
S_m, I_m, and O_m:	Output matrices
ξ_1 and ξ_2:	Noise matrices
P_s:	Population size
ma_i:	The maximum number of iteration
py_i:	The predator presence probability
χ:	The number of decision variables
φ, t:	The gliding constant
s_f:	He scaling factor
ψ_u and ψ_l:	The upper and lower bounds for the decision variable
(η):	Flying squirrels
B_s:	A bell-curved number
$\overline{a}(t)$:	Measurement noise
(QCFs):	Quadratic cost functions
(FV):	Fitness value
(ψ_{at}):	Flying squirrels on acorn nut trees
gl_d:	The gliding distance
ls_c:	The sliding constant

η_{kt}: Flying squirrel on the hickory tree
η_{ot}^{t}: Flying squirrel on a normal tree
pp_p: The predator presence probability
ran_l: Random location
$\text{sea}_{\min}$: Seasonal constant's minimum value
ev_y: Levy distribution function.

Data Availability

Data Available and supported for finding this work. Data collected from various sources and research centres in the area of fuzzy logic control for power systems.

Conflicts of Interest

The authors declare that they have no conflicts of interest.

Acknowledgments

The authors would like to acknowledge all the research scholars belonging to the Engineering and Technology and all the members of the R&D Centre, CMR College of Engineering & Technology, Hyderabad, India, for providing valuable suggestions and essential facilities in completing this work.

References

[1] A. Hosseinipour and H. Hojabri, "Virtual inertia control of PV systems for dynamic performance and damping enhancement of DC microgrids with constant power loads," *IET Renewable Power Generation*, vol. 12, no. 4, pp. 430–438, 2018.

[2] S. Samanta, J. P. Mishra, and B. K. Roy, "Implementation of a virtual inertia control for inertia enhancement of a DC microgrid under both grid connected and isolated operation," *Computers and Electrical Engineering*, vol. 76, pp. 283–298, 2019.

[3] Yi Zhang, Q. Sun, J. Zhou, L. Li, P. Wang, and J. M. Guerrero, "Coordinated control of networked AC/DC microgrids with adaptive virtual inertia and governor-gain for stability enhancement," *IEEE Transactions on Energy Conversion*, vol. 36, no. 1, pp. 95–110, 2021.

[4] O. Azeem, M. Ali, G. Abbas et al., "A comprehensive review on integration challenges, optimization techniques and control strategies of hybrid ac/dc microgrid," *Applied Sciences*, vol. 11, no. 14, pp. 6242–6332, 2021.

[5] Lu Huang and Q. Yu, "Stability analysis of DC microgrid considering the action characteristics of relay protection," in *Proceedings of the 2019 3rd International Conference on Power and Energy Engineering*, Qingdao, China, October 2019.

[6] R. Madurai Elavarasan, A. Ghosh, T. K Mallick, A. Krishnamurthy, and M. Saravanan, "Investigations on performance enhancement measures of the bidirectional converter in PV-wind interconnected microgrid system," *Energies*, vol. 12, no. 14, pp. 2672–2722, 2019.

[7] M. A. N. pashaki, F. Karbalaei, and S. Abbasi, "Optimal placement and sizing of distributed generation with small signal stability constraint," *Sustainable Energy, Grids and Networks*, vol. 23, 2020.

[8] O. A. Ajeigbe, J. L. Munda, and Y. Hamam, "Optimal allocation of renewable energy hybrid distributed generations for small-signal stability enhancement," *Energies*, vol. 12, no. 24, pp. 4777–4831, 2019.

[9] T. He, S. Li, S. Wu, and Ke Li, "Small-signal stability analysis for power system frequency regulation with renewable energy participation," *Mathematical Problems in Engineering*, vol. 2021, Article ID 5556062, pp. 1–13, 2021.

[10] J. Liu, M. J. Hossain, J. Lu, F. Rafi, and H. Li, "A hybrid AC/DC microgrid control system based on a virtual synchronous generator for smooth transient performances," *Electric Power Systems Research*, vol. 162, pp. 169–182, 2018.

[11] B. Bankovic, F. Filipovic, N. Mitrovic, M. Petronijevic, and V. Kostic, "A building block method for modeling and small-signal stability analysis of the autonomous microgrid operation," *Energies*, vol. 13, no. 6, pp. 1492–1528, 2020.

[12] T. K. Renuka, P. Reji, and S. Sreedharan, "An enhanced particle swarm optimization algorithm for improving the renewable energy penetration and small signal stability in power system," *Renewables: Wind, Water, and Solar*, vol. 5, no. 1, pp. 6–17, 2018.

[13] S. M. Malik, Y. Sun, X. Ai, Z. Chen, and K. Wang, "Small signal analysis of a hybrid microgrid with high pv penetration," *IEEE Access*, vol. 4, pp. 1–13, 2016.

[14] T. Santhoshkumar and V. Senthil kumar, "Transient and small signal stability improvement in microgrid using AWOALO with virtual synchronous generator control scheme," *ISA Transactions*, vol. 104, pp. 233–244, 2020.

[15] A. Khodadadi, P. Hasanpor Divshali, M. H. Nazari, and S. H. Hosseinian, "Small-signal stability improvement of an islanded microgrid with electronically-interfaced distributed energy resources in the presence of parametric uncertainties," *Electric Power Systems Research*, vol. 160, pp. 151–162, 2018.

[16] Q. Xu, Y. Xu, C. Zhang, and P. Wang, "A robust droop-based autonomous controller for decentralized power sharing in DC microgrid considering large-signal stability," *IEEE Transactions on Industrial Informatics*, vol. 16, no. 3, pp. 1483–1494, 2020.

[17] C. Prathyusha, M. Vijaya Shanthi, and V. Harish, "Validation of solar PV-wind hybrid system with incremental conductance algorithm," *Journal of Advanced Research in Dynamical and Control Systems*, vol. 12, pp. 1168–1179, 2020.

[18] S. Amirkhan, M. Radmehr, M. Rezanejad, and S. Khormali, "An improved passivity-based control strategy for providing an accurate coordination in a AC/DC hybrid microgrid," *Journal of the Franklin Institute*, vol. 356, no. 13, pp. 6875–6898, 2019.

[19] P. K. Ray and A. Mohanty, "A robust firefly-swarm hybrid optimization for frequency control in wind/PV/FC based microgrid," *Applied Soft Computing*, vol. 85, Article ID 105823, 2019.

[20] S. Merugu, K. Jain, A. Mittal, and B. Raman, "Sub-scene target detection and recognition using deep learning convolution neural networks," in *Proceedings of the 1st International Conference on Data Science, Machine Learning and Applications - ICDSMLA 2020*, pp. 1082–1101, Springer, Singapore, June 2020.

[21] S. Merugu, A. Tiwari, and S. K. Sharma, "Spatial–spectral image classification with edge preserving method," *Journal of the Indian Society of Remote Sensing*, vol. 49, no. 3, pp. 703–711, 2021.

[22] N. Hosseinzadeh, A. Aziz, A. Mahmud, A. Gargoom, and M. Rabbani, "Voltage stability of power systems with renewable-energy inverter-based generators: a review," *Electronics*, vol. 10, no. 2, pp. 115–127, 2021.

[23] H. Shahsavari and A. Nateghi, "Optimal design of probabilistically robust PID controller to improve small signal stability of PV integrated power system," *Journal of the Franklin Institute*, vol. 356, no. 13, pp. 7183–7209, 2019.

[24] H. Kuttomparambil Abdulkhader, J. Jacob, and A. T. Mathew, "Robust type-2 fuzzy fractional order PID controller for dynamic stability enhancement of power system having RES based microgrid penetration," *International Journal of Electrical Power and Energy Systems*, vol. 110, pp. 357–371, 2019.

[25] P. Hassan, M. Radmehr, and M. Rezanejad, "Lypunov theory combined with small signal linearization for regulated operation of a hybrid DC/AC microgrid," *International Transactions on Electrical Energy Systems*, vol. 30, no. 9, 2020.

[26] N. Kumar, I. E. E. E. Senior Member, and S. Kumar Panda, "Fellow ieee A multipurpose and power quality improved electric vessels charging station for the seaports," *IEEE Transactions on Industrial Informatics*, vol. 10, 2020.

[27] A. S. Shaik, R. K. Karsh, M. Suresh, and V. Gunjan, "LWT-DCT based image hashing for tampering localization via blind geometric correction," in *Proceedings of the 2nd International Conference on Data Science, Machine Learning and Applications ICDSMLA*, Springer, Singapore, July 2022.

[28] J. Y. Siu, "IEEE, nishant kumar, senior member, IEEE, and sanjib kumar panda, fellow," *IEEE "Command Authentication Using Multiagent System for Attacks on the Economic Dispatch Problem" IEEE TRANSACTIONS ON INDUSTRY APPLICATIONS*, vol. 58, no. 4, 2022.

[29] P. Negi, Y. Pal, and G. Leena, "Grid-connected photovoltaic system stability enhancement using ant lion optimized model reference adaptive control strategy," *Differential Equations and Dynamical Systems*, 2020.

[30] G. Devadasu and M. Sushama, "Identification of voltage quality problems under different types of Sag/Swell faults with Fast Fourier Transform analysis," in *Proceeding of the IEEE - 2nd International Conference on Advances in Electrical, Electronics, Information, Communication and Bio-Informatics, IEEE – AEEICB*, pp. 464–469, Chennai, India, October 2016.

[31] G. Devadasu and M. Sushama, "A novel multiple fault identification with fast fourier transform analysis," in *Proceedings of the 2016 International Conference on Emerging Trends in Engineering, Technology and Science (ICETETS)*, Pudukkottai, India, October 2016.

[32] N. Kumar, I. E. E. E. Senior Member, and S. Kumar Panda, "Fellow IEEE "smart high power charging networks and optimal control mechanism for electric ships," *IEEE Transactions on Industrial Informatics*, vol. 19, no. 2, 2023.

[33] F. Feng, X. Zhang, J. Zhang, and H. B. Gooi, "Stability enhancement via controller optimization and impedance shaping for dual active bridge-based energy storage systems," *IEEE Transactions on Industrial Electronics*, vol. 68, no. 7, pp. 5863–5874, 2021.

[34] P. Rodriguez, I. Candela, and A. Luna, "Control of PV generation systems using the synchronous power controller," in *Proceedings of the 2013 IEEE Energy Conversion Congress and Exposition*, Denver, CO, USA, October 2013.

[35] A. S. Shaik, R. K. Karsh, M. Islam, and S. P. Singh, "A secure and robust autoencoder-based perceptual image hashing for image authentication," *Wireless Communications and Mobile Computing*, vol. 2022, Article ID 1645658, pp. 1–17, 2022.

[36] B. Chandramouli, A. Vijaya prabhu, D. Arun Prasad, K. Kathiravan, N. Udhayaraj, and M. Vijayasanthi, "Design of single switch-boosted voltage current suppressor converter for uninterrupted power supply using green resources integration," *Electrical Engineering and Electromechanics*, vol. 5, pp. 31–35, 2022.

[37] J. Y. Siu, S. K. Nishant Kumar, and A. Panda, "Detection and mitigation using multi-agent system in the deregulated market," in *Proceedings of the 2021 IEEE 12th Energy Conversion Congress and Exposition - Asia (ECCE-Asia)*, Singapore, May 2021.